J. Fluid Mech. (1994), *vol.* 277, *pp.* 1–21

Structure of turbulent boundary layers on smooth and rough walls

By P.-Å. KROGSTAD[1] AND R. A. ANTONIA[2]

[1] Division of Mechanics, Thermo- and Fluid Dynamics, Norwegian Institute of Technology, N-7034 Trondheim, Norway

[2] Department of Mechanical Engineering, University of Newcastle, NSW, 2308, Australia

(Received 6 September 1993 and in revised form 28 March 1994)

The structure of turbulent boundary layers which develop with zero pressure gradient on a smooth wall and a k-type rough wall was examined using arrays of X-wires. Although the data were obtained only on two orthogonal planes, the technique provides some information on the three-dimensionality of the large-scale structures. The major effect of the roughness is to tilt the inclination of the structures towards the wall-normal direction. This is caused by the reduced damping of the wall-normal velocity fluctuations close to the rough surface and the break-up of structures whose scales are comparable to the size of the roughness elements. Both effects cause a reduction in the streamwise lengthscales, as suggested by all the measured two-point correlations. The correlations also show that the roughness tends to reduce the overall anisotropy of the large-scale motion. There is evidence to suggest that the magnitude of the vorticity field is larger over the rough wall.

1. Introduction

The effect of surface roughness on turbulent boundary layers usually results in an increase in surface skin friction. It has been assumed (e.g. Rotta 1962; Hinze 1975; Raupach, Antonia & Rajagopalan 1991) that this effect is primarily felt in the 'roughness sublayer', of the order of a few roughness heights away from the wall. As the roughness effect is expected to be confined to the wall region, the mean velocity and turbulent stresses in the outer layer should be very little affected. Based on this assumption, Hama (1954) concluded that the velocity defect function for a smooth surface also applies to the flow over a rough wall. This similarity has later been assumed to exist and has been used to estimate the value of the skin friction coefficient, C_f, in a number of experiments (Furuya & Fujita 1967; Bandyopadhyay 1987; Perry, Lim & Henbest 1987) since this quantity is not readily available when the surface is rough. An exact velocity defect similarity for smooth and rough surface flows should lead to identical distributions of $U_e^+ - U^+$ as function of $y^* = y/\delta$, except very close to the wall. (Here U denotes the mean velocity in the streamwise direction and the superscript $^+$ denotes normalization by the friction velocity, $u_\tau = (\tau_w/\rho)^{1/2}$.) Consequently, the dependence of the Reynolds stress $\overline{u_i^+ u_j^+}$ on y^* should also be similar for the two flows.

On the basis of differences observed between turbulent boundary layers over a smooth surface and a surface roughened by a mesh screen, the previous similarity was questioned by Krogstad, Antonia & Browne (1992*a*). Pimenta, Moffat & Kays (1979) had also challenged this similarity on the basis of Reynolds stress data obtained over a rough surface consisting of copper balls which had been brazed together into a

uniformly permeable wall. The much higher C_f over a rough surface implies a faster growth rate of the layer. Therefore a different entrainment rate should be expected which will manifest itself in a stronger 'wake' component, implying differences in the mean velocity as well as in the Reynolds stress profiles in the outer layer. Using an optimization technique for curve fitting the data obtained in the mesh screen rough-wall boundary layer, Krogstad *et al.* found a value of $\Pi \approx 0.7$ for the strength of the 'wake' component, compared to $\Pi = 0.52$ which is implicit in the Hama defect function. The high value of Π for the rough surface is in accord with the earlier findings of Osaka & Mochizuki (1988) and Tani (1988) for a boundary layer on a *d*-type rough wall (a series of spanwise square bars, separated by square cavities).

The difference in mean velocity characteristics in the outer layer suggests that the interaction between the inner and the outer regions is stronger than is normally assumed. This would in turn imply that differences should also exist for turbulence quantities, not only in the wall region, but also in the outer layer. The measurements of Perry *et al.* (1987), Acharya & Escudier (1987) and Krogstad *et al.* (1922*a*) all show that the streamwise normal stress $\overline{u^{+2}}$ is primarily affected in the wall region and remains virtually unaffected in the outer region. The difference near the surface is caused by the differences in the turbulent energy production in this region. Large effects were, however, reported for $\overline{v^{+2}}$ (Acharya & Escudier; Krogstad *et al.*). Krogstad *et al.* showed that these differences were caused by an increase in the energy content at high wavenumbers in the rough-wall case. They also found that the surface roughness affected the Reynolds shear stress $-\overline{u^+v^+}$ in the outer layer as well as in the inner layer. The contributions to the second and fourth quadrants of the (u, v)-plane were increased nearly everywhere in the layer.

The previous observations suggest that there may be a more effective communication between the wall region and the outer region than has been assumed hitherto. (Such a possibility was considered, albeit speculatively, by Antonia 1972.) This also implies that there may be differences in the large-scale motions for these two flows. These possibilities are explored further in this paper through the use of arrays of X-wires which cover a significant portion of the boundary-layer thickness. This approach has previously been used in the far wake of a cylinder (Bisset, Antonia & Browne 1990) and in a smooth-wall boundary layer (Antonia *et al.* 1990*a*).

Flow patterns in the planes of the arrays can be visualized and the corresponding data can be treated in a number of ways to provide quantitative information about the large-scale motions. One approach is to compute conventional space–time correlations, which may be used to infer a physical picture of the large-scale motion, as previously illustrated by Townsend (1976) and Grant (1958). Another approach is to condition the information in the planes of the arrays on a feature (or features) of the large-scale motion (e.g. Antonia, Bisset & Browne 1990*a*). Both approaches have been adopted in the present work, the results in the smooth-wall layer providing a basis of comparison for the rough wall. Also, the use of orthogonal arrays in the rough-wall boundary layer allows three-dimensional aspects of the large-scale motion to be examined.

2. Experimental set-up

The experiments were carried out in an open return wind tunnel with a 5.2 m long test section and a cross-section of 800 mm × 160 mm.

The smooth-surface experiment was carried out at a free-stream velocity, U_e, of 10.9 m s^{-1}. At the measurement station, 4.3 m from the end of the tunnel contraction, the friction velocity, u_τ, was 0.42 m s^{-1} and the boundary-layer thickness, δ, was

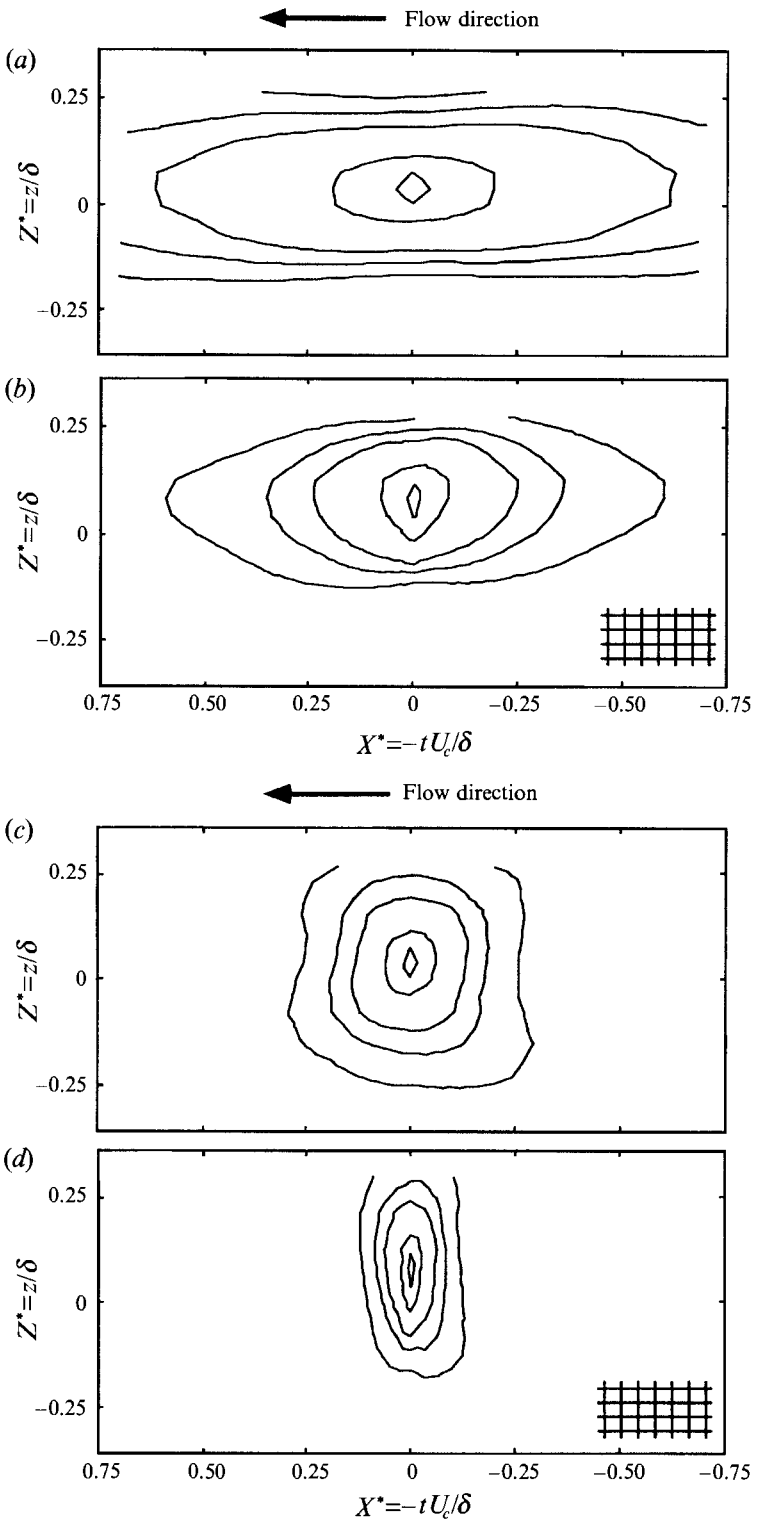

FIGURE 1. Isocontours of ρ_{uu} and ρ_{ww} in the (x, z)-plane at $y_0^* = y_0/\delta \approx 0.24$. Contours: 0.1, 0.2, 0.3, 0.6, 0.9. ρ_{uu}: (*a*) smooth; (*b*) rough. ρ_{ww}: (*c*) smooth; (*d*) rough. Grid gives approximate mesh spacing.

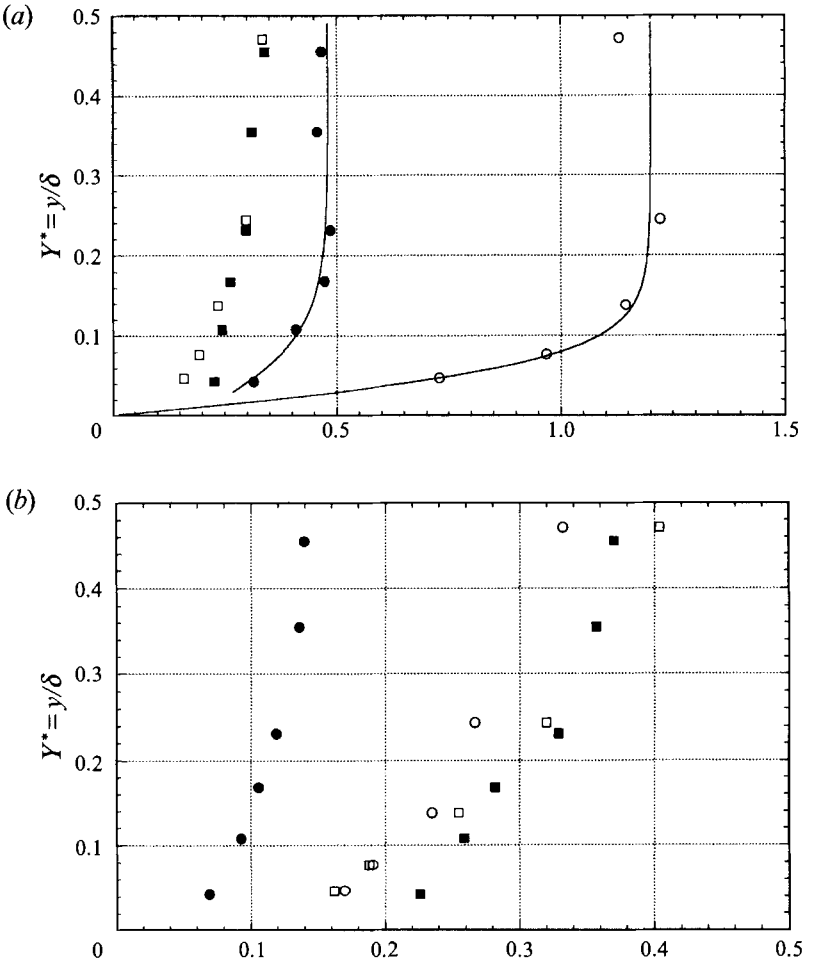

FIGURE 2. Streamwise and spanwise lengthscales associated with correlations in the (x, z)-plane. Δx^*: ●, rough; ○, smooth; Δz^*: ■, rough; □, smooth. (*a*) $\rho_{uu} = 0.3$, ——, $\Delta x^* \sim \tanh(12y^*)$; (*b*) $\rho_{ww} = 0.3$.

66 mm. The momentum thickness, θ, was 8.3 mm, and the Reynolds number $R_\theta = U_e\theta/\nu$ was 6030; note that this Reynolds number is well beyond the range for which low-Reynolds-number effects are normally assumed to be important. Full details of the set-up and flow characteristics are given by Antonia *et al.* (1990*a*). An array of eight equally spaced X-wire probes was used for the velocity measurements. The array could be positioned either perpendicular to the wall to measure u and v, or parallel to the surface to measure u and w. In the (x, y)-plane the array spanned the range 0.02δ to 0.55δ, while for the experiments in the (x, z)-plane, the array covered $\pm 0.27\delta$.

The rough surface consisted of a woven stainless steel mesh screen with a wire diameter $d = 0.69$ mm ($d^+ = 46$, $d/\delta \approx 0.009$) and a spacing $t = 3.18$ mm ($t^+ = 212$, $t/\delta \approx 0.042$). The screen was attached to the test wall over a distance of 3.5 m, starting at the beginning of the test section. The origin for y was taken in the plane of the screen crests. (The effective origin was approximately 0.4 mm below this plane; see Krogstad *et al.* 1992*a* for further details.) The wall opposite the rough surface was adjusted to achieve a zero pressure gradient. The free-stream velocity was 20 m s^{-1}. At the measurement station, 2.46 m from the end of the tunnel contraction, u_τ was 1.0 m s^{-1}

and δ was 75 mm. The momentum thickness θ was 9.92 mm, and $R_\theta \simeq 12800$. Full details of the set-up and flow characteristics are given in Krogstad & Browne (1991); Krogstad *et al.* (1992*a*) found that the characteristics of the rough wall correspond to a sand grain roughness with $k_s = 4.96$ mm ($k_s^+ = 331$, $k_s/\delta \approx 0.066$).

For the rough-surface experiments, the instrumentation was extended. Sixteen X-wire probes were used simultaneously, arranged in two mutually orthogonal arrays, each containing eight X-wires. The X-wires in the vertical array were in the (x, y)-plane and were arranged to measure u and v. The horizontal array was in the (x, z)-plane, with probes arranged to measure u and w. The X-wires of both arrays were located at the same streamwise position. In this way, measurements could be obtained simultaneously in the two planes.

The nominal separation between probes in the vertical array was 4.4 mm ($\Delta y/\delta \approx 0.06$), so that the overall distance covered by the array was 0.41δ. This array was mounted on a traverse which allowed it to be positioned anywhere within the layer and moved to the free stream for calibration. The horizontal array was mounted on a separate traverse mechanism. The design was such that the horizontal array was divided into two almost identical halves. The nominal probe separation in each half of this array was 5 mm although, to make room for the vertical array, the central probes were separated by ± 7 mm. The spanwise extent of the horizontal array was $\pm 0.30\delta$. Further details about this experiment are given by Krogstad, Antonia & Browne (1993).

Although the spacing between the probes was much too large to allow correct estimates of the fluctuating vorticity and strain rates, it was expected that the calculation of these quantities would, none the less, allow a useful comparison between the large-scale motions in the two boundary layers. For this purpose, the vorticities $\omega_y = \partial u/\partial z - \partial w/\partial x$ and $\omega_z = \partial v/\partial x - \partial u/\partial y$, as well as the strain rates $s_{xy} = \partial u/\partial y + \partial v/\partial x$ and $s_{xz} = \partial w/\partial x + \partial u/\partial z$ were computed. Gradients in the streamwise distance were obtained using Taylor's hypothesis $\partial/\partial x \approx -U_c^{-1}\partial/\partial t$, where U_c is the turbulent convection velocity, here taken to be the local mean velocity, and the time derivative was estimated using central differences. In the direction across the array, gradients were obtained by first fitting a cubic spline to the instantaneous velocity data from all the probes at any particular time and then calculating the derivatives.

3. Two-point correlations

Using the data from the arrays, conventional two-point correlation coefficients for the streamwise and lateral velocity fluctuations were calculated in the (x, y)- and (x, z)-planes. Two-point coefficients are defined by

$$\rho_{pq}(\boldsymbol{x}_0, \boldsymbol{x}, \tau) = \frac{\overline{p(\boldsymbol{x}_0, t)\, q(\boldsymbol{x}, t+\tau)}}{p' q'},$$

where p and q represent velocity fluctuations (u, v or w), $\boldsymbol{x}_0$ (components x_0, y_0, z_0) denotes the vector location of the reference probe and $\boldsymbol{x} = \boldsymbol{x}_0 + \Delta\boldsymbol{x}$ is the location of the other probe. One would not expect ρ_{pq} to depend on either x_0 or z_0 if homogeneity is valid in these directions. It may however depend strongly on y_0 (and y), as previously noted, for example by Kovasznay, Kibens & Blackwelder (1970).

Correlation results in the (x, z)-plane were obtained at seven y_0 locations from $y_0^* = y_0/\delta = 0.017$ to 0.47 for the smooth wall and at eight positions from 0.043 to 0.46 for the rough wall. The results will be presented for the reference location $y_0^* \simeq 0.23$,

i.e. roughly in the middle of the range covered in both cases. The time delay τ was converted to a streamwise distance with Taylor's hypothesis, i.e. $x^* = x/\delta = -\tau U_c/\delta$. The flow direction is right to left in all plots. The convection velocity was chosen to be the mean velocity at the reference probe location; U_c/U_e was 0.76 and 0.64 for the smooth and rough walls, respectively. The correlations obtained from the arrays were first checked by comparing them with autocorrelations computed from single probe data obtained at a much higher sampling rate (and, for the smooth wall case, at a Reynolds number which was twice as large, i.e. at roughly the same Reynolds number as for the rough wall). No significant differences were found.

Figures 1 and 2 indicate that there are similarities as well as differences in the correlation patterns for the two flows. The variation of the spanwise (Δz^*) and streamwise (Δx^*) lengthscales, which are associated with the maximum widths (along the z- and x-directions, respectively) of the contours $\rho_{uu} = 0.3$ and $\rho_{ww} = 0.3$ obtained with the array parallel to the surface, is shown in figure 2 as a function of the distance from the wall. (These ρ-levels were chosen as a reasonable compromise in order to focus on the large-scale events, while still maintaining sufficiently accurate correlations.) There is a significant difference in the magnitude of Δx^* for the two flows; this is independent of y^*. This difference is also large compared to the lengthscales of the surface roughness ($t/\delta \approx 0.042$). The spanwise extent of the correlations is about the same in the two cases, both for ρ_{uu} and ρ_{ww}. For $y^* < 0.2$, the width of the smooth wall correlations decreases more rapidly than for the rough wall. This is consistent with the observation that the lengthscales, e.g. the mixing length, are smaller near a smooth than a rough surface (Rotta 1962). For comparison, lines have been added (figure 2*a*) with the same general shape as the mixing length model of Michel, Quemard & Durant (1968), i.e.

$$\Delta x^* = \Delta x_0^* + k_1 \tanh(k_1 y^*).$$

The lengthscales decrease to zero as the smooth wall is approached. For the rough wall, they decrease to a finite length determined by the lengthscales of the surface roughness. For the smooth wall, the streamwise extent of the correlations (ρ_{uu} and ρ_{ww}) is larger than that on the rough wall by a factor of more than two.

For isotropic turbulence, the ratio of the major axes, i.e. $\Delta x^*/\Delta z^*$ for ρ_{uu}, should be equal to 2 (e.g. Frenkiel 1948). As originally noted by Grant (1958), the correlations for the smooth surface are highly anisotropic. The ratio $\Delta x^*/\Delta z^*$ (calculated from ρ_{uu}) decreased from about 5 near the wall to 3 at $y^* \approx 0.5$. For ρ_{ww}, the ratio $\Delta z^*/\Delta x^*$ remained constant ($\simeq 1.1$) in the domain covered by the measurements. For the rough surface, the ratio $\Delta x^*/\Delta z^*$ (inferred from ρ_{uu}) decreased from 3.2 near the wall to 2.6 at $y^* \approx 0.15$ and remained nearly constant at larger y^*. As for the smooth surface, the ratio $\Delta z^*/\Delta x^*$ (inferred from ρ_{ww}) was nearly constant, although with a slightly larger magnitude ($\simeq 1.5$). Both ρ_{uu} and ρ_{ww} thus indicate a tendency towards isotropy caused by the surface roughness. For isotropy, one would expect that the z-extent of ρ_{ww} should be equivalent to the x-extent of ρ_{uu}. For the present range of y^*, the ratio $\Delta x^*/\Delta z^*$ was in the range 1.3 to 1.7 for the rough wall ($\rho_{uu} = \rho_{ww} = 0.3$). For the smooth wall, this ratio decreased almost linearly from 5.5 at $y^* = 0.047$ to 2.8 at $y^* = 0.47$. All these results suggest that, in the context of the gross features of the large-scale motion, isotropy is more nearly approximated over the rough-wall than in the smooth-wall layer. Support for this tendency is also provided by the magnitudes of Reynolds stresses (Krogstad *et al.* 1992*a*). While in the outer part of the layer $\overline{u^{+2}}$ was virtually unaffected by the surface roughness, $\overline{v^{+2}}$ and $\overline{w^{+2}}$ both increased by more than 30% in the region covered by the probe arrays.

Contours of the two-point vorticity correlation coefficient (figure 3) also exhibit

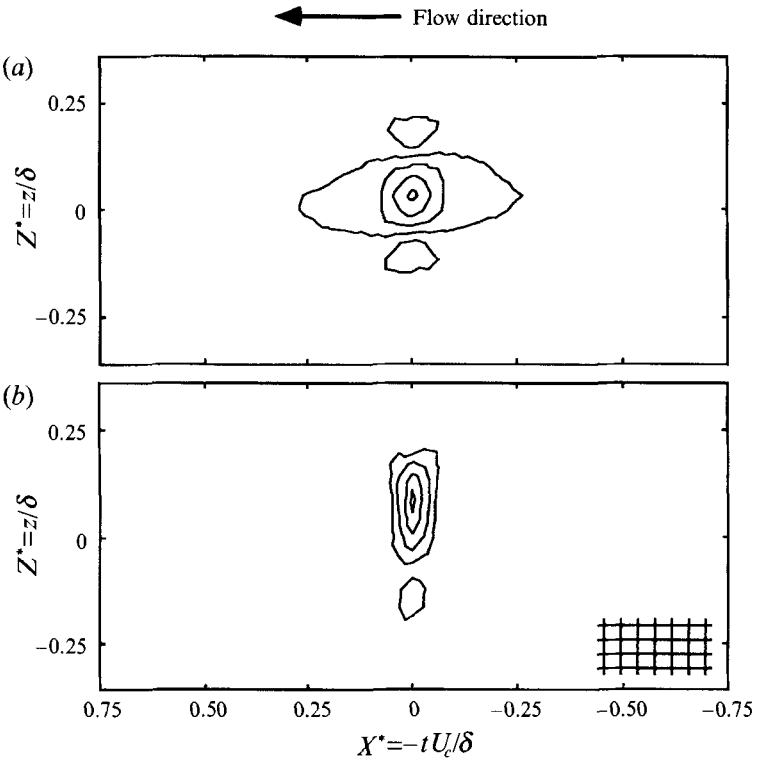

FIGURE 3. Isocontours of $\rho_{\omega_y\omega_y}$ in the (x,z)-plane at $y_0^* \approx 0.24$. Contours: -0.1, 0.1, 0.3, 0.6, 0.9; (*a*) smooth; (*b*) rough.

significant differences between the two surfaces. The scales of the axes are the same as in figure 1, thus highlighting the large difference in lengthscales between vorticity and velocity. The streamwise extent of the correlations is clearly much larger for the smooth surface. The distributions across the layer of the streamwise and lateral correlation lengths associated with $\rho_{\omega_y\omega_y} = 0.3$ and $\rho_{s_{xz}s_{xz}} = 0.3$ are shown in figure 4. The streamwise extent of the correlations is considerably shorter over the rough than over the smooth surface. On the other hand, the lateral extent is much larger over the rough surface. There is, however, very little difference between the lengthscales associated with ω_y and s_{xz}. The smooth-surface contours are almost circular while the rough-wall contours are more extended in the lateral than in the streamwise direction. For both rough and smooth walls, there are distinct negative correlation regions on either side of the correlation peak, indicating that vortical motion in the (x,y)-plane is, on average, flanked by counter-rotating fluid. (On the rough wall, the lateral correlation length was too large relative to the size of the array to allow the negative regions to be detected on both sides. However, when the correlation function at $x^* = 0$ was plotted against z^*, it became apparent that a negative zone must also be present for $z^* > 0.3$.)

The tendency for the streamwise extent of all correlations to be greater for the smooth than for the rough wall, is consistent with the largescale structures being, on average, less inclined to the smooth wall than to the rough wall. This is in accord with the observation by Krogstad *et al.* (1992*a*) that $\overline{v^{+2}}$ is increased over the rough wall owing to the less efficient damping of vertical motions near the surface. Also, because of the interaction with the roughness elements, it is unlikely that elongated streamwise vortical structures will form near the wall. Based on flow visualizations and spanwise

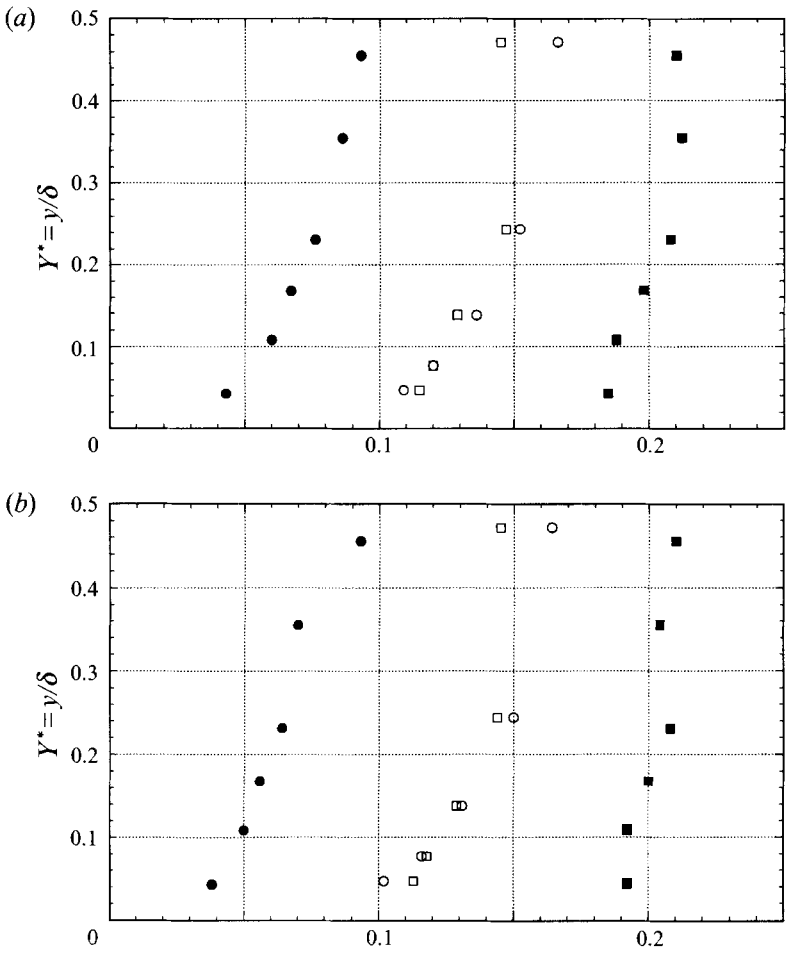

FIGURE 4. Streamwise and spanwise lengthscales associated with correlations in the (x, z)-plane. (Symbols as in figure 2.) (*a*) $\rho_{\omega_y \omega_y} = 0.3$; (*b*) $\rho_{s_{xz} s_{xz}} = 0.3$.

wavelength spectra obtained close to the surface elements, Grass, Stuart & Mansour-Tehrani (1993) showed that the roughness elements are very efficient in imparting their own lengthscale characteristics to the turbulent flow. These effects result in stronger correlations normal to the wall, but weaker streamwise correlations relative to a smooth surface.

The difference in structure inclination can be more directly inferred from correlations in the (x, y)-plane. For the ρ_{uu} contours in figure 5, the reference probe is at $y^* \simeq 0.16$. (Correlations were also calculated for other reference positions. However, when the reference probe was very close to the surface, the correlation with the outermost probe signal was too low to provide useful information about the inclination. Similarly, if the reference probe was too far from the wall, the correlation near the wall was very weak. These effects were clearly illustrated in Antonia *et al.* 1990*b*. The reference position which was selected seemed to be a reasonable compromise.) The convection velocity U_c at this location was $0.72U_e$ and $0.58U_e$ for the smooth and rough walls, respectively. On the smooth wall, the $\rho_{uu} = 0.3$ contour is inclined at an average angle of about 10° to the wall, in the range $0.1 < y^* < 0.4$. This value is comparable to that ($\simeq 15°$) obtained by Dumas (1989) for the slope of the locus of the maximum correlation (at

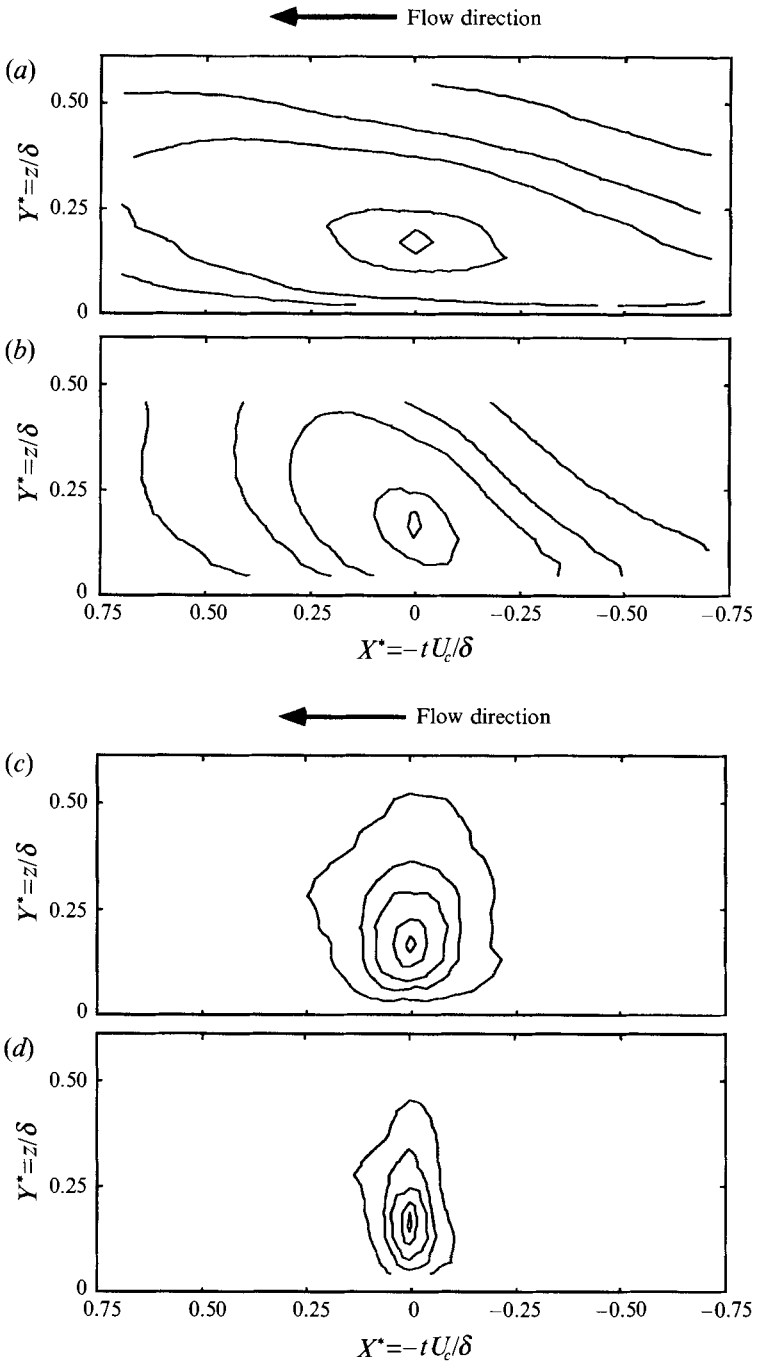

FIGURE 5. Two-point correlations in the (x, y)-plane. Contours: 0.1, 0.2, 0.3, 0.6, 0.9. ρ_{uu}: (*a*) smooth, (*b*) rough; ρ_{vv}: (*c*) smooth, (*d*) rough.

the optimum time delay) in a smooth-wall boundary layer. Over the rough wall, the inclination is about 38°. The streamwise extent of the correlations is about twice as large for the smooth wall as for the rough wall, which is consistent with the (x, z)-plane observations.

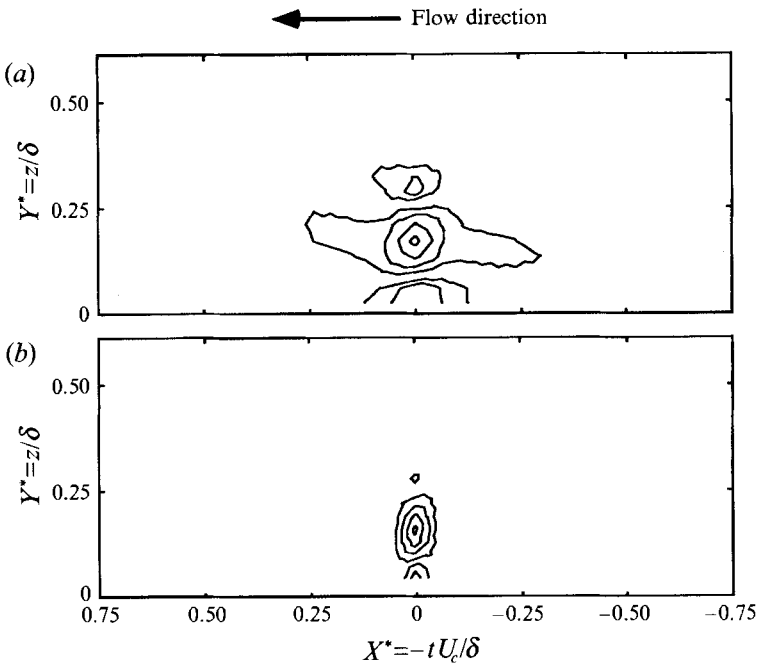

FIGURE 6. Isocontours of $\rho_{\omega_z\omega_z}$ in the (x,y)-plane. Contours: -0.2, -0.1, 0.1, 0.3, 0.6, 0.9; (*a*) smooth; (*b*) rough.

The y-extent of the ρ_{vv} contours (figure 5*c*, *d*) is slightly larger for the smooth wall than for the rough wall. For both surfaces, the spatial extent of ρ_{vv} is considerably smaller than that of ρ_{uu}, owing to the damping effect of the wall on the v fluctuations. However, below the reference point, the correlations are stronger for the rough wall, again reflecting the reduced damping effect of the wall in this case. The contours of ρ_{vv} are more or less aligned in the y-direction, as previously noted for smooth-wall shear layers (e.g. Kovasznay *et al.* 1970; Kim & Hussain 1992). The y-alignment reflects that observed for two-point pressure correlation contours (Kim 1989; Kim & Hussain 1992) although the y-extent of the latter is significantly greater than for ρ_{vv}.

The close similarity of the $\rho_{\omega_z\omega_z}$ and $\rho_{s_{xy}s_{xy}}$ contours in the (x,y)-plane reflects that previously noted for the (x,z)-plane. The spatial extent of $\rho_{\omega_z\omega_z}$ (figure 6) is considerably smaller than for ρ_{uu}. The streamwise lengthscale associated with $\rho_{\omega_z\omega_z}$ is comparable to that for ρ_{vv}, but the y-lengthscale of $\rho_{\omega_z\omega_z}$ is smaller. The average inclination to the wall of the ω_z contours is greater over the rough than the smooth wall, reflecting the difference already noted in connection with the ρ_{uu} contours. The positive correlations near y_0 are flanked by regions of negative correlations above and below the reference point. The regions containing ω_z vorticity therefore appear to be closely associated with regions of opposite-signed vorticity.

The patterns in figure 6(*a*) are qualitatively similar to those obtained by Kim & Hussain (1992) from direct numerical simulation data for a channel flow when the reference location was quite close to the wall ($y_0^+ \simeq 12$). These authors commented on the strong resemblance between the $\rho_{\omega_z\omega_z}$ patterns and the internal shear layers (e.g. Johansson, Alfredsson & Kim 1991).

The negative vorticity regions which lie between the main (positive) vorticity zone and $y = 0$, particularly near the smooth wall, are probably associated with the no-slip condition at the wall (the $\rho_{\omega_z\omega_z}$ contours of Kim & Hussain also display a negative zone

near the wall, consistent with the no-slip condition). In view of the relatively large value of y_0, interpretation of the ω_z patterns in figure 6 in terms of internal shear layers and the no-slip condition seems tenuous. It is possible however that relatively strong spanwise vortices can induce spanwise vorticity of opposite sign near their upper and lower boundaries, especially when the local mean velocity gradient is relatively weak (as would be the case when y_0 is sufficiently large).

4. Conditional results

In order to detect the large-scale structures, the array data were analysed using the window average gradient (WAG) detection scheme (Antonia & Fulachier 1989; Antonia *et al.* 1990*a*). This method is well suited for detecting the discontinuities in the u or v signals which characterize the large-scale motion. WAG searches for changes in the average signal level over a certain time interval. This interval is selected so that the corresponding lengthscale is comparable to the boundary-layer thickness. A window of $2\tau+1$ samples is moved through the data and the quantity

$$\mathrm{WAG}_i = \frac{sign}{2\tau}\left(\sum_{j=i+1}^{i+\tau} u_j - \sum_{j=i-\tau}^{i-1} u_j\right)$$

is computed at every point. A detection begins when WAG_i first exceeds a threshold ku' and ends when WAG_i next becomes negative. The detection point is taken where WAG_i is largest within this interval. The parameter *sign*, taken to be either $+1$ or -1, determines whether the detections will be made for strong accelerations or decelerations.

The present detections were based on strong transitions from negative to positive values of u using a threshold $k = 0.4$ and a window $\tau U_e/\delta = 0.9$. For both surfaces, the resulting average detection frequency was about the same as that obtained using the quadrant method of Lu & Willmarth (1973) for strong Q2 events (quadrant 2 in the (u,v)-plane; threshold $H = 2.5$ and grouping time $T^+ = 55$). The average WAG frequency was practically independent of y^* (for both surfaces) when $y^* \gtrsim 0.1$. In this region, the average time between detections, $\overline{\Delta T}$, when normalized by U_τ and δ, is about 0.16 for the smooth wall and 0.19 for the rough wall. It appears reasonable to expect that, over the span covered by the array, detections made at different y^* are associated with the same structures. Except possibly for the probe closest to the wall, the detections that will be obtained from the various probes of the array in the (x,y)-plane should therefore be strongly correlated.

In order to test this, a correlation function for the detections from the different probes was constructed. An on–off detection function $D(t)$ is defined as follows:

$$D(t) = \begin{cases} 1 & \text{when a detection occurs,} \\ 0 & \text{otherwise.} \end{cases}$$

The correlation coefficient associated with $D(t)$ is given by

$$R_{i,j}(\tau) = \overline{D_i(t)\,D_j(t+\tau)}/D_i' D_j',$$

where

$$\overline{D_i(t)\,D_j(t+\tau)} = \lim_{T\to\infty} \frac{1}{2T}\int_{-T}^{T} D_i(t)\,D_j(t+\tau)\,\mathrm{d}t,$$

$$D_i' = \left(\lim_{T\to\infty} \frac{1}{2T}\int_{-T}^{T} D_i(t)\,\mathrm{d}t\right)^{1/2}.$$

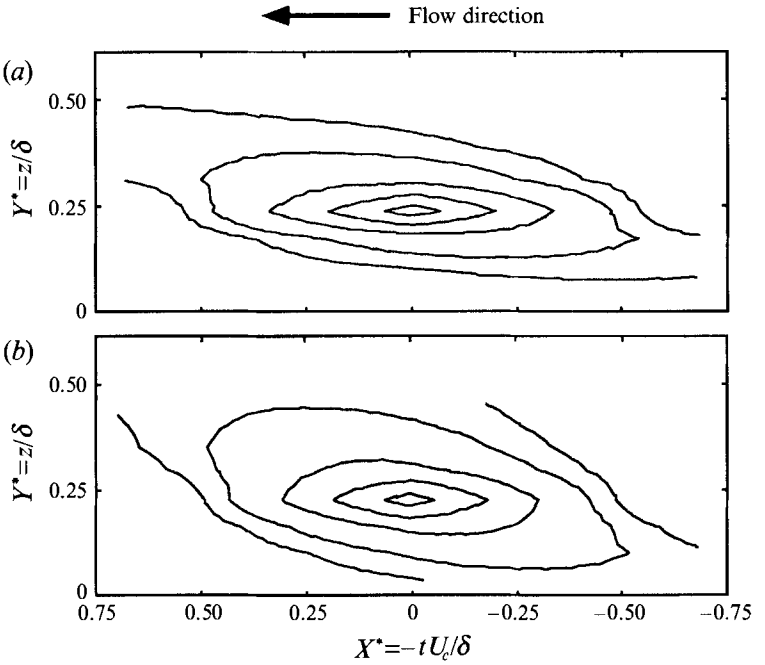

FIGURE 7. Correlations of WAG detections in the (x,y)-plane. Contours: 0.2, 0.3, 0.5, 0.7, 0.9; (*a*) smooth; (*b*) rough.

With this definition D_i' can be interpreted as the r.m.s. value of a digital on–off signal, since $D_i(t) \equiv D_i^2(t)$. The WAG algorithm identifies a detection at the point where the WAG_i function is maximum. Thus, no information about the duration of the event is obtained. Contributions to the two-point correlations are therefore only obtained when the detections are made at exactly the specified τ. Since the probability of this occurrence is very low when the sampling rate is high, the correlation function will contain very few data. To increase the amount of data used for calculating the averages, the duration of the detection was extended upstream and downstream of this point over a distance corresponding to half the length of the WAG window, i.e. $\tau U_e/\delta = 0.45$. In this way the streamwise extent of the correlation function obtained was about the same as for the ρ_{uu} correlations shown in figure 5. The choice of the distance marked as a detection affected the extent of the correlations, but the general shape remained unchanged. Therefore the value used for this parameter does not affect the following observations. Using the probe at $y^* \approx 0.23$ as reference, the correlation functions for the two surfaces are shown in figure 7. (Again the convection velocities were $U_c/U_e = 0.76$ and 0.64 for the smooth and rough walls, respectively.) As for the conventional velocity correlations, ρ_{uu}, of figure 5, the detections indicate that the inclination is steeper on the rough than on the smooth surface. Above the reference point, the inclinations are about 33° (rough) and 15° (smooth). These are in good agreement with the average slopes of the ρ_{uu} contours (38° and 10°, respectively). Closer to the surface, the inclination is less steep in both cases, commensurate with the smaller convection velocity near the wall.

On the basis of the WAG detections, conditional averages were constructed using the techniques described in Krogstad *et al.* (1993). For all the results presented here, the detections were based on the u signal, since this was available in both the (x,y)- and (x,z)-planes and therefore allowed the same type of detections in these planes. 2845

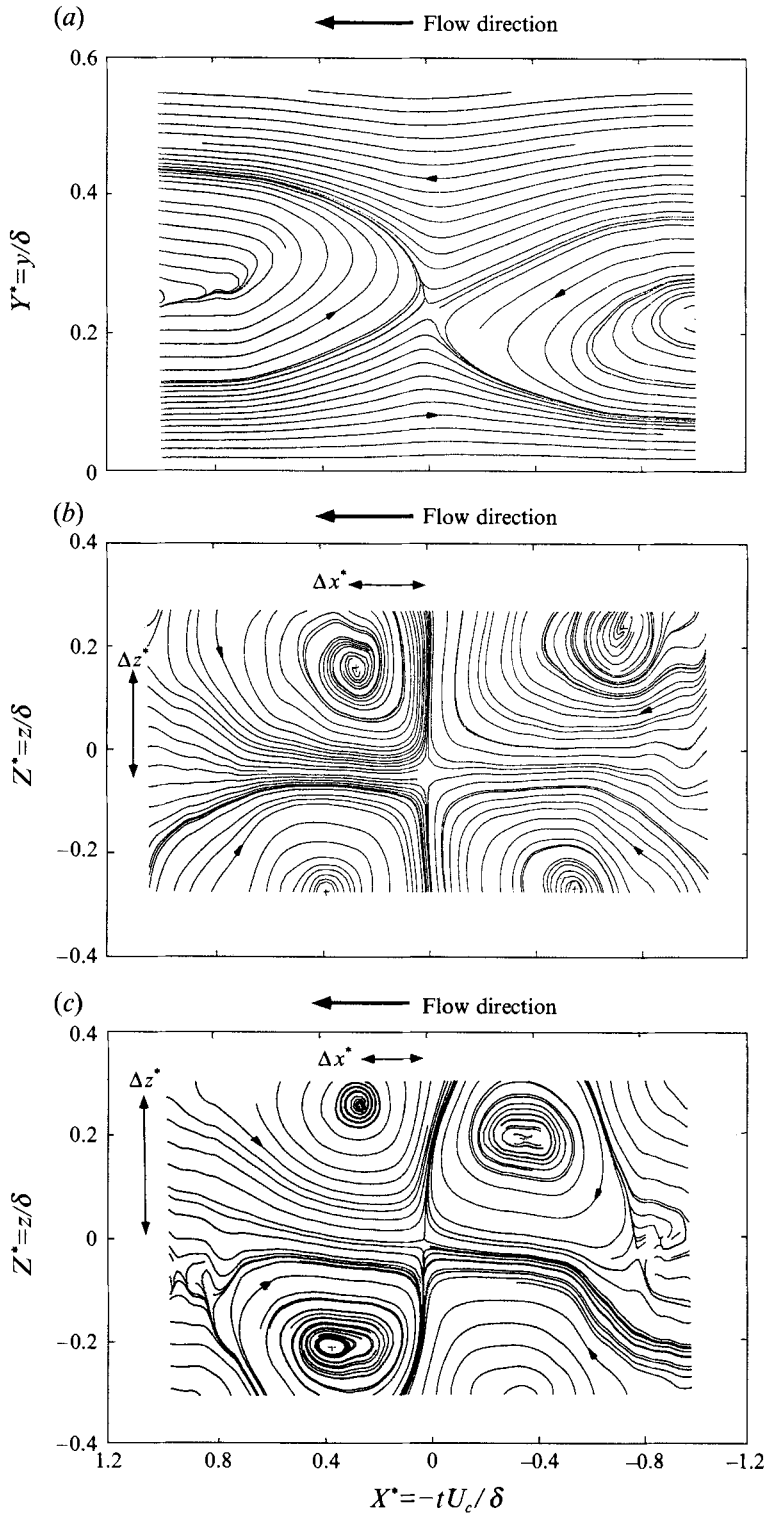

FIGURE 8. Conditional sectional streamlines. For the smooth surface, WAG detections at $x_0^* = 0$, $y_0^* = 0.24$ were used. (*a*) (x, y)-plane; (*b*) (x, z)-plane at $y_0^* = 0.24$. For the rough surface, WAG detections at $x_0^* = 0$, $y_0^* = 0.23$ were used. (*c*) (x, z)-plane at $y_0^* = 0.23$.

detections were made for the rough surface, while the smooth wall produced 754 detections. From these detections, the conditionally averaged velocities in the vicinity of the detection points were generated, as seen by an observer following the flow at a velocity U_c; i.e.

$$\langle u \rangle = U_c - U - \frac{1}{N} \sum_{i=1}^{N} u_i,$$

$$\langle v \rangle = \frac{1}{N} \sum_{i=1}^{N} v_i.$$

N is the number of detections and U the local mean velocity. (V, the local mean velocity normal to the main flow direction, was neglected.) From the set of conditionally averaged velocities, streamlines could be constructed using the method of Bisset *et al.* (1990).

In the (x, z)-plane, the detecting probe was located as close to the array centre as possible. For the smooth surface, this meant using a probe located at $z^* \approx -0.04$, i.e. just off the centreline of the array. For the rough wall, the detection point could be located exactly at the centre of the array by using the probe from the array in the (x, y)-plane. Hence, for the rough wall, conditional averages could be made in both planes based on identical detections.

Figure 8 shows conditional streamlines obtained in the two planes for the smooth surface. In the (x, y)-plane (figure 8*a*), the streamlines are based on detections obtained from the probe located at $y_0^* = 0.24$. ($x^* = 0$ denotes the detection point.) The streamlines reflect a strong upward motion downstream of the detection point ($x^* > 0$), followed by a wall-directed motion ($x^* < 0$). This is a consequence of detecting a strong transition from a low to a high value of u. (An almost identical set of streamlines was found for the rough surface.) In the (x, z)-plane (figure 8*b*), the flow pattern is reminiscent of four vortical-like motions centred around the detection point ($x^* = 0$ and $z^* = -0.042$). The high-speed inrushing fluid which overtakes the slow-speed ejection in the (x, y)-plane causes a strong divergence in the (x, z)-plane. This produces the vortical motions centred on the two upstream focal points located at $x^* \approx -0.6$ and -0.8. The downstream, slower moving fluid causes a motion with an opposite direction of rotation as the high-speed fluid moves around it. This flow is centred at the two foci located at $x^* \approx 0.3$ and 0.4, i.e. about half the distance from the point of detection compared to the upstream pair. The same type of pattern was observed for the rough surface (figure 8*c*) although the foci in this case were at different locations with respect to the detection point. This is especially true for the upstream foci which are much closer to the detection point than in the smooth case.

On the assumption that the relative locations of the foci contain some information about the size of the dominant structures, the distance between foci in the (x, z)-plane was determined for different values of y_0^*. Figure 9(*a*) shows that the spanwise separation, Δz^*, between the two foci downstream of the detection point is larger on the rough than on the smooth surface. (This also applies to the separation between the upstream foci.) For the smooth wall, Δz^* agrees well with the spanwise scales computed by Antonia & Bisset (1991). Close to the surface, the difference appears to be largest, although here the results may be somewhat unreliable, since the distance between the probes in the array becomes comparable to the separation of the foci whose locations are therefore difficult to determine precisely. Allowing for this uncertainty, the separation between the foci is at least 50% larger for the rough than for the smooth wall at $y^* \approx 0.05$.

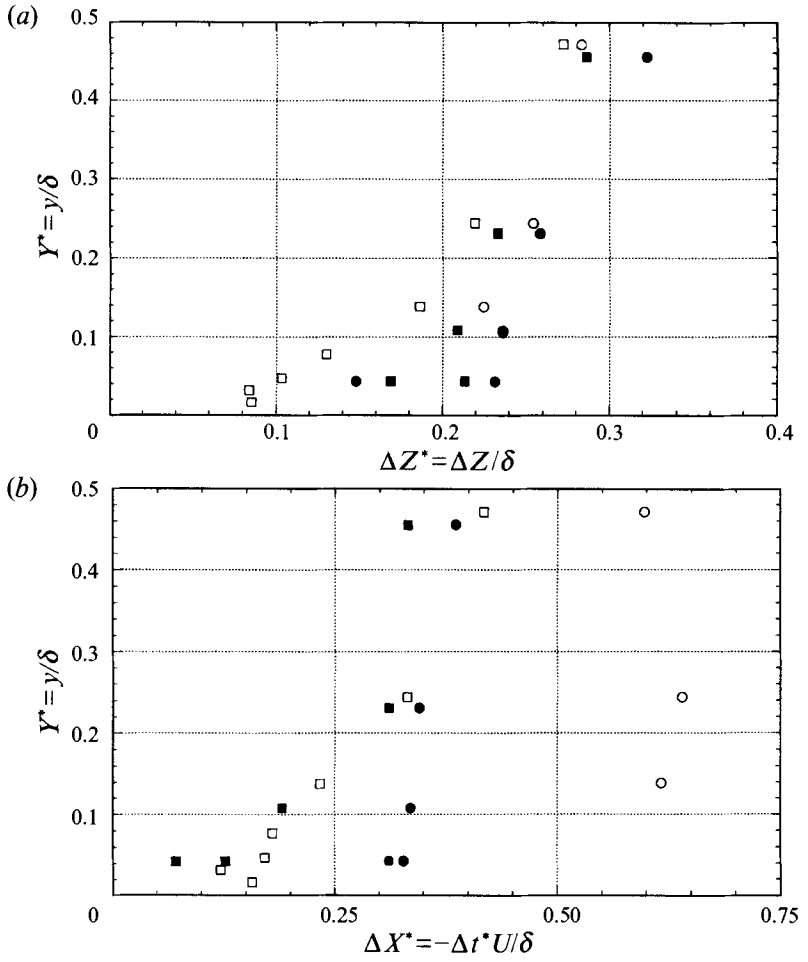

FIGURE 9. Separation between foci inferred from sectional streamlines in the (x,z)-plane based on WAG detections. Rough: ●, upstream foci; ■, downstream foci. Smooth: ○, upstream foci; □, downstream foci. (*a*) Spanwise separation; (*b*) streamwise separation.

Figure 9(*b*) shows the streamwise positions of the foci. This distance, Δx^*, has been defined as the mean distance from the detection point to the two downstream or upstream foci, respectively. The main difference between the two surfaces is reflected in the location of the upstream foci, which is about twice as large for the smooth wall as for the rough wall. The location of the two downstream foci appears to be the same in both cases, except perhaps very near the wall. Since the downstream foci are associated with ejection-like motions while the upstream foci are related to sweep-like motions, the differences in the locations of the upstream foci appear to reflect the stronger v damping of the sweep-like motions by the smooth wall and the weaker lengthscales for u over the rough wall. There is a striking difference between the dependence of the upstream and downstream foci on y^*. The location of the upstream foci is almost independent of y^* for both surfaces. For the rough wall, the ratio $\Delta x^*/\Delta z^*$ is nearly unity, while it is quite large near the smooth wall. The differences in the locations of foci generally mirror the earlier observations based on the correlations, i.e. the spanwise widths are about the same, but there are considerable differences in the streamwise direction.

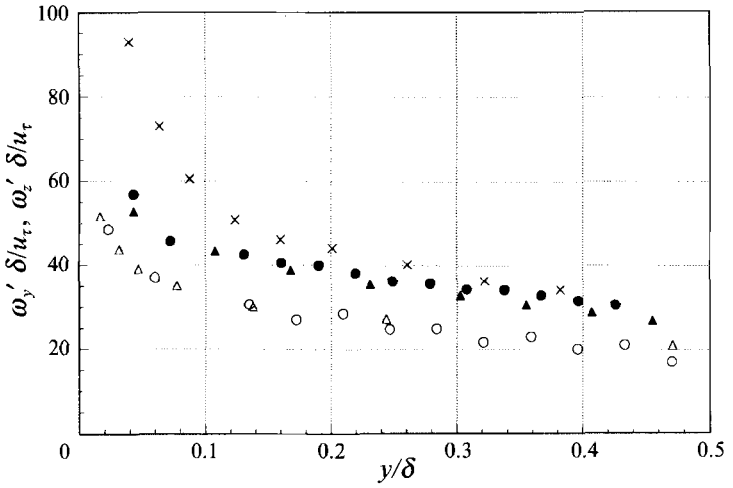

FIGURE 10. Root mean square vorticity distributions. $\omega_y'\delta/u_\tau$: ▲, rough; △, smooth; $\omega_z'\delta/u_\tau$: ●, rough; ○, smooth; ×, Rajagopalan & Antonia 1993.

The components ω_y and ω_z of the vorticity vector are of interest since the Reynolds shear stress gradient is explicitly linked to the correlations $\overline{v\omega_z}$ and $\overline{w\omega_y}$ through the identity (e.g. Tennekes & Lumley 1972; Hinze 1975)

$$-\partial(\overline{uv})/\partial y = \overline{v\omega_z} - \overline{w\omega_y} + 1/2\,\partial(\overline{u^2} - \overline{v^2} - \overline{w^2})/\partial x.$$

The contributions from the streamwise derivative term is expected to be small (e.g. Klewicki 1989; Antonia & Rajagopalan 1990). Figure 10 shows distributions of the conventional r.m.s. values for ω_y' and ω_z'. Also included are values of ω_z' which were measured in a smooth-wall boundary layer at $R_\theta = 1450$ (same wind tunnel) with a four-wire vorticity probe of adequate spatial resolution (Rajagopalan & Antonia 1993; these authors noted that these values were in reasonable agreement with the measurements of Balint, Wallace & Vukoslavcevic 1991 and Klewicki & Falco 1990). As may be seen from the definitions of the vorticities (see §2) the result will depend to some extent on the choice of convection velocity used in Taylor's hypothesis. The distributions in figure 10 were obtained using $U_c = U(y)$. The use of $U_c = 0.75U(y)$ yielded a 14.5% increase in ω_z', while $U_c = 1.25U(y)$ resulted in a 7% reduction in ω_z'. These variations are relatively small compared with the differences in ω_z' between the two flows. Kim & Hussain (1992) found, using the channel flow DNS data, that U seemed to be the correct propagation velocity for the vorticity fluctuations, except near the surface. One would expect that the ambiguity associated with the use of U as the convection velocity in the (x, z)-plane should be small so that the effect of Taylor's hypothesis should be smaller on ω_y' than ω_z'.

As expected, the present values of ω_z' (and ω_y') are underestimated, especially near the wall, owing to the poor spatial resolution of the arrays. Accordingly, the present data are not of sufficient quality to provide reliable data for the velocity/vorticity correlations in the previous identity. (A four-wire vorticity probe should be used for this purpose; these measurements are planned for the future.) Nevertheless, the present data for ω_y' and ω_z' are useful for the purpose of comparison since they were obtained with similar spatial resolutions in both layers. Over the domain of the probe array, ω_y' and ω_z' are approximately equal in each layer, which is consistent with the observations of Balint *et al.* (1991) in a smooth-wall layer. However, for the rough surface, ω_y' and

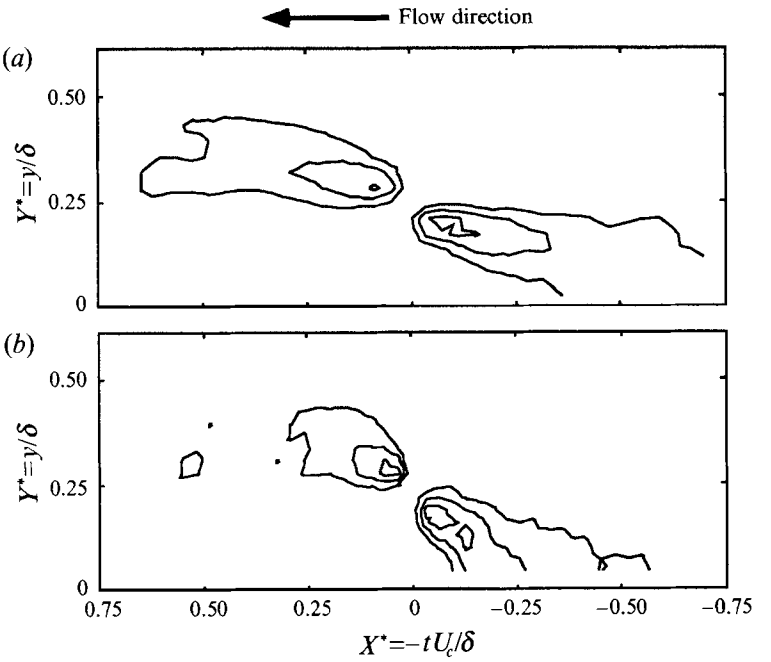

FIGURE 11. Conditional vorticity $\langle\omega_z\rangle\,\delta/u_\tau$ in the (x,y)-plane. WAG detections at $x_0^* = 0$, $y_0^* \approx 0.24$ were used. (Only negative vorticity is shown.) Contours: -5, -10, -15; (*a*) smooth; (*b*) rough.

ω_z' are consistently higher (30–40 %) than for the smooth wall. Almost the same increase (25–40 %) was found for s_{xy}' and s_{xz}'. This increase is supported by the increases in $-\overline{u^+v^+}$ and $\overline{v^{+2}}$ (Krogstad *et al.* 1992*a*).

Distributions of $\langle\omega_z\rangle\,\delta/u_\tau$ in the (x,y)-plane are shown in figure 11 for the two flows. Near the detection point, the distributions are similar, reaching about the same peak value. The smooth-wall contours are relatively elongated relative to the rough-wall contours. Also, the inclination is different; near the detection location, it is about 33° for the rough wall and 12° for the smooth wall; these values are consistent with previous estimates of the inclinations.

For the rough wall, velocity data in the two planes were available simultaneously. Therefore, some information about the three-dimensionality of the flow can be obtained. Instantaneous flow patterns in the two planes were reported in Krogstad *et al.* (1992*b*, 1993). Structural features which occur simultaneously in the two planes were identified. Based on quadrant detections in the (x,y)-plane, both co- and counter-rotating structures existed simultaneously in the two halves of the (x,y)-plane. Statistical analysis showed that counter-rotating structures were most probable.

Here, WAG detections were made at y_0^*, a fixed (reference) location in the (x,y)-plane, while the array in the (x,z)-plane was traversed to different y^* locations, keeping the x- and z-locations fixed. Conditionally averaged results in the (x,z)-plane were then obtained, the probe in the (x,y)-array at $y_0^* = 0.23$ being the reference probe. Conditional data were obtained in the (x,z)-plane for the range $0.04 < y^* < 0.46$. This enabled the streamwise variation in the locations of the foci relative to the detection point ($x^* = 0$) to be mapped out as a function of y^*. The streamwise positions of the saddle points at the centreline and the position of the upstream and downstream foci are shown in figure 12, together with the contours for the conditional strain $\langle s_{xy}\rangle\,\delta/u_\tau$. A close correlation between these quantities is expected because s_{xy} is one of the

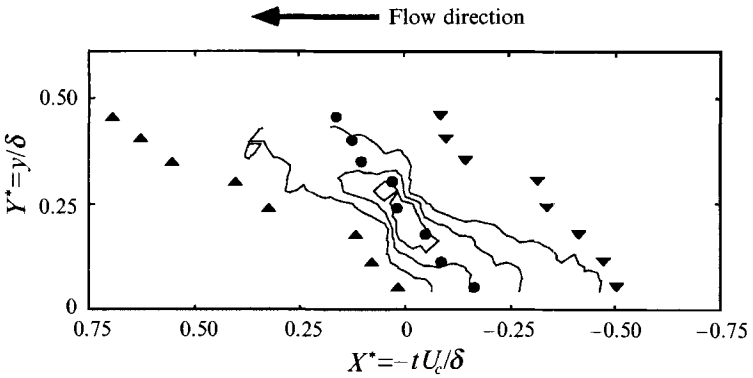

FIGURE 12. Conditional strain rate $\langle s_{xy}\rangle \delta/u_\tau$ in the (x,y)-plane for the rough surface. WAG detections at $x_0^* = 0$, $y_0^* \approx 0.24$ were used. (Only positive strain rate is shown.) Contours: 5, 10, 15. ●, saddle point; ▲, downstream foci; ▼, upstream foci.

principal components responsible for vortex stretching in the (x,y)-plane. In the vicinity of y_0^*, the locus of the saddle points is in close alignment with the locus of the maximum conditional strain rate. The locations of the foci vary almost linearly with y^*; this variation suggests constant inclinations of about 31° and 43° for the downstream and upstream foci respectively. The average of these two values agrees closely with the average slope of about 38° which was inferred from the conventional two-point u correlations of §3. The steeper inclination of the locus of upstream foci compared with that of the locus of downstream foci is also supported by the rough-wall two-point correlation data estimated by Krogstad *et al.* (1993) on the basis of quadrant detections. These authors concluded that Q4 events were inclined at a larger angle to the wall than Q2 events. WAG concentrates on rapid jumps between low and high values of u and therefore focuses on transitions between ejections and sweeps. Since Q4 events are associated with sweeps, these events would be expected to be closely related to the motion on the upstream side of WAG detections.

5. Concluding discussion

The effect of surface roughness on the structure of a turbulent boundary layer has been examined and compared with corresponding results for a smooth-wall layer. The data for both layers were obtained using arrays of eight X-wires in planes which were either parallel or/and normal to the surface. The results indicate that the major structural difference between the two layers is associated with the average inclination to the wall of the large-scale structures. Over the smooth wall, this inclination is less than half that on the rough wall. Strong support for this difference was provided by a relatively detailed set of conventional two-point correlations in either the y- or z-direction. Data conditioned on a particular feature of the large-scale motion (the detection method focused on a relatively sudden and spatially coherent change in the longitudinal velocity fluctuation) corroborated the conclusions drawn from the correlations. Despite the fact that two-point correlations are generally thought to be weak indicators of the flow fields associated with organized motions (e.g. Raupach *et al.* 1991), the present conventional correlations provide fairly reliable information on the major (three-dimensional) features of the large-scale motion, apparently without significant degradation by less organized aspects of the motion.

It is worth commenting on the impact different boundary conditions can have on the

extent and shape of the correlation contours. An analogy may be drawn between the effect of introducing a surface roughness and that caused by wall transpiration. For example, Sano & Hirayama (1986) observed a significant contraction – relative to the reference (zero transpiration) state – of u correlation contours in the outer part of a boundary layer when injection was applied through a two-dimensional wall slit. The application of suction through the slit resulted in an appreciable expansion of the contours. A significant increase in the spatial characteristics of the large-scale motion was also found by Antonia & Fulachier (1989) when a relatively small suction rate was applied uniformly at the surface. These observations tend to suggest that there is relatively efficient transfer of information between the wall and the outer region of a turbulent boundary layer. The spatial extents of the correlations appear to reflect the boundary condition in a sensitive manner.

Commensurate with the smaller inclination to the wall of the large-scale structures, the longitudinal lengthscale is considerably larger on a smooth than on a rough wall. However, the spanwise extent of the motion is about the same in the two cases. Conventional r.m.s. values of the strain rates in the (x,y)- and (x,z)-planes were noticeably larger for the rough-wall layer. Similarly, the r.m.s. values of the wall-normal and spanwise components of the vorticity are discernibly bigger over the rough wall. These results, which need to be confirmed by measurements with better spatial resolution, tend to imply increased stretching and amplification of the vortices. This would be consistent with the earlier speculation (Krogstad *et al.* 1992*a*) that the active motion, which should account for nearly all the Reynolds shear stress in the inner region of the layer, is also intensified by the introduction of the roughness. The present data are also consistent with the observation by Grass (1971) that ejections over a rough wall can be relatively violent, the ejected fluid rising almost vertically into the outer flow and often remaining identifiable through much of the flow.

Overall, it would appear that the primary effect of surface roughness is to change the shape of the large-scale motion, although we have evidence suggesting that the strength of this motion may also be increased. These changes appear to be partly associated with the increased intensity of the wall-normal velocity fluctuations. In this way, the surface roughness is found to reduce the overall anisotropy of the flow. Partial evidence for this is provided by the considerably smaller difference between the normal stresses over the rough than on the smooth wall. Also, the two-point correlations over the rough wall are in closer agreement with isotropy than the smooth-wall correlations.

It is likely that the roughness generates new vortical structures with scales comparable to those of the roughness elements. This suggestion is supported by the observation (Grass *et al.* 1993) of a dominant spanwise wavelength close to a k-type roughness. These authors noted that this wavelength, which reflects the typical scale of near-wall vortical structures, is proportional to the size of the roughness elements. They also observed that horseshoe-type vortical structures were as dominant in the rough-wall layer as in the smooth-wall layer and that the scale of these structures increased with distance from the wall. The present data for the large-scale vortical structures seem compatible with the possible existence of (usually asymmetrical) horseshoe-like vortices. Conventional vorticity correlations and conditional streamlines in the (x,z)-plane support this possibility, notwithstanding the artificial symmetry in that plane. The data also appear to be consistent with the inverted double cone wall-attached eddies proposed by Townsend (1976). The wall inclination of these structures should be greater for the rough wall than for the smooth wall; on the basis of the z-span of the present correlation contours, the average diameter of these structures should increase with distance from the wall.

It is appropriate to comment on the generality of the present results, given that a wide range of parameters can come into play when describing a particular type of surface roughness. One parameter is the ratio δ/k; the present value of δ/k ($\simeq 50$) is typical of roughnesses encountered in the laboratory so that the present results should be generally relevant. As noted in Krogstad *et al.* (1992*a*), the present surface may be described as a k-type roughness (sand-grain roughness is of this type) which is the one usually encountered in both laboratory and atmospheric flows (see the review of Raupach *et al.* 1991). It should, however, be recalled that the three-dimensionality of the roughness cannot be discounted (Raupach *et al.*). To date, the classification of rough walls has been based solely on the effect the roughness has on the mean velocity. This is clearly insufficient; the present results, as well as those from previous investigations (for references, see Krogstad *et al.* 1992*a*), indicate that a roughness classification in terms of turbulence structure would be worth pursuing in the future. Further, the present results, even if they are strictly applicable to geometrically similar rough walls, suggest that future kinematic models of the large-scale structure of a turbulent boundary layer will need to reflect the effect of the surface condition.

R.A.A. is grateful to the Australian Research Council for its support.

REFERENCES

ACHARYA, M. & ESCUDIER, M. 1987 Turbulent flow over mesh roughness. In *Turbulent Shear Flows 5* (ed. F. Durst, B. E. Launder, J. L. Lumley, F. W. Schmidt & J. H. Whitelaw), pp. 176–185. Springer.

ANTONIA, R. A. 1972 Conditionally sampled measurements near the outer edge of a turbulent boundary layer. *J. Fluid Mech.* **56**, 1–18.

ANTONIA, R. A. & BISSET, D. K. 1991 Three-dimensional aspects of the organized motion in a turbulent boundary layer. In *Turbulence and Coherent Structures* (ed. O. Métais & M. Lesieur), pp. 141–157. Dordrecht: Kluwer.

ANTONIA, R. A., BISSET, D. K. & BROWNE, L. W. B. 1990*a* Effect of Reynolds number on the organized motion in a turbulent boundary layer. *J. Fluid Mech.* **213**, 267–286.

ANTONIA, R. A., BROWNE, L. W. B. & BISSET, D. K. 1990*b* Effect of Reynolds number on the organized motion in a turbulent boundary layer. In *Near-Wall Turbulence* (ed. S. J. Kline & N. H. Afgan), pp. 488–506. Hemisphere.

ANTONIA, R. A. & FULACHIER, L. 1989 Topology of a turbulent boundary layer with and without wall suction. *J. Fluid Mech.* **198**, 429–451.

ANTONIA, R. A. & RAJAGOPALAN, S. 1990 Performance of lateral vorticity probe in a turbulent wake. *Exps Fluids* **9**, 118–120.

BALINT, J.-L., WALLACE, J. M. & VUKOSLAVCEVIC, P. 1991 The velocity and vorticity vector fields of a turbulent boundary layer. Part 2. Statistical properties. *J. Fluid Mech.* **228**, 53–86.

BANDYOPADHYAY, P. R. 1987 Rough-wall turbulent boundary layers in the transitional regime. *J. Fluid Mech.* **180**, 231–266.

BISSET, D. K., ANTONIA, R. A. & BROWNE, L. W. B. 1990 Spatial organization of large structures in the turbulent far wake of a cylinder. *J. Fluid Mech.* **218**, 439–461.

DUMAS, R. 1989 Observations on the boundary layer based on measured correlations with various improvements. In *Near-Wall Turbulence* (ed. S. J. Kline & N. H. Afgan), pp. 437–452. Hemisphere.

FRENKIEL, F. N. 1948 On the kinematics of turbulence. *J. Aero. Sci.* **52**, 57–64.

FURUYA, Y. & FUJITA, H. 1967 Turbulent boundary layers on a wire-screen roughness. *Bull. JSME* **10**, 77–86.

GRANT, H. L. 1958 The large eddies of turbulent motion. *J. Fluid Mech.* **4**, 149–190.

GRASS, A. J. 1971 Structural features of turbulent flow over smooth and rough boundaries. *J. Fluid Mech.* **50**, 233–255.

GRASS, A. J., STUART, R. J. & MANSOUR-TEHRANI, M. 1993 Common vortical structure of turbulent flows over smooth and rough boundaries. *AIAA J.* **31** (5), 837–847.

HAMA, F. R. 1954 Boundary layer characteristics for smooth and rough surfaces. *Trans. Soc. Naval Arch. Marine Engrs* **62**, 333–358.

HINZE, J. O. 1975 *Turbulence*, 2nd edn. McGraw-Hill.

JOHANSSON, A. V., ALFREDSSON, P. H. & KIM, J. 1991 Evolution and dynamics of shear-layer structures in near-wall turbulence. *J. Fluid Mech.* **224**, 579–599.

KIM, J. 1989 On the structure of pressure fluctuations in simulated turbulent channel flow. *J. Fluid Mech.* **205**, 421–451.

KIM, J. & HUSSAIN, F. 1992 Propagation velocity and space–time correlation of perturbations in turbulent channel flow. *NASA TM* 103932.

KLEWICKI, J. C. 1989 Velocity–vorticity correlations related to the gradients of the Reynolds stresses in parallel turbulent wall flows. *Phys. Fluids* A **1**, 1285–1288.

KLEWICKI, J. C. & FALCO, R. E. 1990 On accurately measuring statistics associated with small-scale structure in turbulent boundary layers using hot-wire probes. *J. Fluid Mech.* **219**, 119–142.

KOVASZNAY, L. S. G., KIBENS, V. & BLACKWELDER, R. F. 1970 Large-scale motion in the intermittent region of a turbulent boundary layer. *J. Fluid Mech.* **41**, 283–326.

KROGSTAD, P.-Å., ANTONIA, R. A. & BROWNE, L. W. B. 1992*a* Comparison between rough- and smooth-wall turbulent boundary layers. *J. Fluid Mech.* **245**, 599–617.

KROGSTAD, P.-Å., ANTONIA, R. A. & BROWNE, L. W. B. 1992*b* Structure investigation in a turbulent boundary using orthogonal X-wire arrays. In *Proc. 11th Australasian Fluid Mech. Conf. Hobart, Tasmania* (ed. M. R. Davis & G. J. Walker), pp. 251–254.

KROGSTAD, P.-Å., ANTONIA, R. A. & BROWNE, L. W. B. 1993 The use of orthogonal X-wire arrays for structure investigation in a turbulent boundary layer. *Exps Fluids* **15**, 231–239.

KROGSTAD, P.-Å. & BROWNE, L. W. B. 1991 Turbulent boundary layer flow over a rough surface. *Rep. TN FM* 91/1, Department of Mechanical Engineering, University of Newcastle, Australia.

LU, S. S. & WILLMARTH, W. W. 1973 Measurements of the structure of the Reynolds stress in a turbulent boundary layer. *J. Fluid Mech.* **60**, 481–511.

MICHEL, R., QUEMARD, C. & DURANT, R. 1968 Hypotheses on the mixing length and application to the calculation of the turbulent boundary layers. In *Proc. Computation of Turbulent Boundary Layers* (ed. S. J. Kline, M. V. Morkovin, G. Sovran & D. J. Cockrell). Stanford.

OSAKA, H. & MOCHIZUKI, S. 1988 Coherent structure of a *d*-type rough wall boundary layer. In *Transport Phenomena in Turbulent Flows: Theory, Experiment and Numerical Simulation* (ed. M. Hirata & N. Kasagi), pp. 199–211. Hemisphere.

PERRY, A. E., LIM, K. L. & HENBEST, S. M. 1987 An experimental study of the turbulence structure in smooth- and rough-wall boundary layers. *J. Fluid Mech.* **177**, 437–466.

PIMENTA, M. M., MOFFAT, R. J. & KAYS, W. M. 1979 The structure of a boundary layer on a rough wall with blowing and heat transfer. *J. Heat Transfer* **101**, 193–198.

RAJAGOPALAN, S. & ANTONIA, R. A. 1993 RMS spanwise vorticity measurements in a turbulent boundary layer. *Exps Fluids* **14**, 142–144.

RAUPACH, M. R., ANTONIA, R. A. & RAJAGOPALAN, S. 1991 Rough-wall turbulent boundary layers. *Appl. Mech. Rev.* **44**, 1–25.

ROTTA, J. C. 1962 Turbulent boundary layers in incompressible flow. *Prog. Aero. Sci.* **2**, 1–219.

SANO, M. & HIRAYAMA, N. 1986 The structure of the outer intermittent region of turbulent boundary layers with injection and suction through a slit. *Bull. JSME* **29**, 2469–2475.

TANI, I. 1988 Turbulent boundary layer development over rough surfaces. In *Perspectives in Turbulence Studies* (ed. H. U. Meier & P. Bradshaw), pp. 223–249. Springer.

TENNEKES, H. & LUMLEY, J. L. 1972 *A First Course in Turbulence*. MIT Press.

TOWNSEND, A. A. 1976 *The Structure of Turbulent Shear Flow*, 2nd edn. Cambridge University Press.